Version 03 as of February 4, 2020
Primary authors: Carlos Yero, Werner Boeglin, Mark Jones
To be submitted to PRL
Comment to cyero002@fiu.edu by xxx, yyy

First Measurements of the D(e,e'p)n Cross Section at Very High Recoil Momenta and Large Q^2

C. Yero and W.U. Boeglin
Florida International University, University Park, Florida 33199, USA

M.K. Jones
Thomas Jefferson National Accelerator Facility, Newport News, Virginia 23606, USA

(for the Hall C Collaboration)
(Dated: February 4, 2020)

New $^2H(e,e'p)n$ cross sections have been measured at 4-momentum transfers of $Q^2 = 4.5 \pm 0.5$ $(\mathrm{GeV/c})^2$ reaching neutron recoil (missing) momenta up $p_r \sim 1.01$ GeV/c. The data have been obtained at fixed neutron recoil angles $\theta_{nq} = 35^\circ$ and 45° with respect to the 3-momentum transfer, $\vec{q}$. At these kinematic settings final state interactions (FSI), meson exchange currents (MEC) and isobar configurations (IC) are expected to be suppressed and the plane wave impulse approximation (PWIA) provides the dominant cross section contribution. The new data are compared to recent theoretical calculations where a significant disagreement at very high missing momenta has been observed.

The deuteron is the only bound two-nucleon system and serves as a starting point to study the strong nuclear force at the subfermi distance scale, a region which is currently not well understood. At such small internucleon distances the nucleon-nucleon (NN) interaction is expected to become repulsive and the interacting nucleons begin to overlap. This short distance region is directly related to two-nucleon short range correlations (SRC) observed in $A > 2$ nuclei [1–4]. Short-range studies of the deuteron are also important in determining whether or to what extent the description of nuclei in terms of nucleon/meson degrees of freedom is still valid before having to include explicit quark degree of freedoms, an issue of fundamental importance in nuclear physics[5]. As of the present time, there are only a few nuclear physics experiments for which a transition between nucleonic to quark degrees of freedom has been observed [6–8].

The most direct way to study the short range structure of the deuteron wave function (or equivalently, its high momentum components) is via the exclusive deuteron electro-disintegration reaction at very high neutron recoil (or missing) momenta. Within the plane wave impulse approximation (PWIA), the virtual photon couples to the bound proton which is subsequently ejected from the nucleus without further interaction with the recoiling system (neutron). The neutron carries a momentum equal in magnitude but opposite in direction to the initial state proton, $\vec{p}_r = -\vec{p}_{i,p}$, thus providing information on the momentum of the bound nucleon and its momentum distribution. In reality, the ejected nucleon undergoes final state interactions (FSI) corresponding to subsequent interactions with the recoiling system. Another possibility is that the photon couples to the virtual meson being exchanged between nucleons (meson exchange currents), or that the photon excites a bound nucleon into a resonance state which subsequently decays back into its ground state (isobar configurations). FSI, meson exchange currents (MEC) and isobar configurations (IC) can significantly alter the recoiling neutron momentum thereby obscuring the original momentum of the bound nucleon and reducing the possibility of directly probing the deuteron momentum distribution.

Theoretically, MEC and IC are expected to be suppressed at $Q^2 > 1$ $(\mathrm{GeV/c})^2$) and Bjorken $x_{Bj} \equiv Q^2/2M_p\omega > 1$, where M_p and ω are the proton mass and photon energy transfer, respectively. The suppression of MEC can be understood from the fact that the estimated MEC scattering amplitude is proportional to $(1+Q^2/m^2_{meson})^{-2}(1+Q^2/\Lambda^2)^{-2}$, where $m_{meson} \approx 0.71$ $(\mathrm{GeV/c})^2$ and $\Lambda^2 \sim 0.8-1$ $(\mathrm{GeV/c})^2$[9]. IC can be suppressed kinematically by selecting $x_{Bj} > 1$, where one probes the lower energy part of the deuteron quasi-elastic peak which is maximally far away from the inelastic resonance electro-production threshold.

Previous deuteron electro-disintegration experiments performed at lower Q^2 ($Q^2 < 1$ $(\mathrm{GeV/c})^2$)[See Section 5 of Ref. [10]] have helped quantify the contributions from FSI, MEC and IC on the $^2H(e,e'p)n$ cross-section and to determine the kinematics at which they are either suppressed (MEC and IC) or under control (FSI).

At large Q^2, FSI are described by the General Eikonal

Approximation (GEA)[9–11] which predicts a strong dependence of FSI on neutron recoil angles θ_{nq}. GEA predicts FSI to be maximal for $\theta_{nq} \sim 70^o$. This strong angular dependence has been found to lead to the cancellation of FSI at neutron recoil angles around $\theta_{nq} \sim 40^o$ and $\theta_{nq} \sim 120^o$. Since at $\theta_{nq} \sim 120^o$ IC are not negligible, $x_{Bj} > 1$ and, equivalently, $\theta_{nq} \sim 40^o$ is the preferred choice to suppress IC as well as FSI.

The first $^2H(e,e'p)n$ experiments at high Q^2 were carried out at Jefferson Lab (JLab) in Halls A[12] and B[13]. Both experiments determined that the cross-sections for fixed missing momenta indeed exhibited a strong angular dependence with neutron recoil angles peaking at $\theta_{nq} \sim 70^o$ in agreement with GEA[9, 11] calculations. In Hall B, the CEBAF Large Acceptance Spectrometer (CLAS) measured angular distributions for a range of Q^2 values as well as momentum distributions. However, statistical limitations made it necessary to integrate over a wide angular range to determine momentum distributions which are therefore dominated by FSI, MEC and IC for missing momenta above ~ 300 MeV/c.

In Hall A, the pair of high resolution spectrometers (HRS) made it possible to measure the missing momentum dependence of the cross section for fixed neutron recoil angles (θ_{nq}) reaching missing momenta up to $p_r = 550$ MeV/c. For the first time very different momentum distributions were found for $\theta_{nq} = 35 \pm 5^o$ and 45 ± 5^o compared to $\theta_{nq} = 75 \pm 5^o$. Theoretical models attributed this difference to the suppression of FSI at the smaller angles ($\theta_{nq} = 35, 45^o$) compared to FSI dominance at $\theta_{nq} = 75^o$[14].

The experiment presented in this Letter takes advantage of the kinematic window previously found in the Hall A experiment and extends the $^2H(e,e'p)n$ cross section measurements to $Q^2 = 4.5 \pm 0.5$ (GeV/c)^2 and neutron recoil momenta up to 1.01 GeV/c. At the selected kinematic settings with neutron recoil angles between 35^o and 45^o, MEC and IC are suppressed and FSI are under control giving access to high momentum components of the deuteron wave function.

A 10.6 GeV electron beam was incident on a 10 cm long liquid deuterium target (LD2). The scattered electron and knocked-out proton were detected in coincidence by the new Super High Momentum Spectrometer (SHMS) and the High Momentum Spectrometer (HMS), respectively. The recoiling neutron was reconstructed using energy-momentum conservation. The missing momentum is defined as $\vec{p_r} = \vec{q} - \vec{p_f}$ and the missing energy as $E_m = \omega - T_p - T_r$ where $\vec{p_f}$ is the final proton momentum, $\vec{q}$ is the 3-momentum transfer and (T_p and T_r) are the final proton and neutron kinetic energies respectively. The beam currents delivered by the accelerator ranged between 45-60 μA and the beam was rastered over a 2x2 mm^2 area to reduce the effects of localized boiling on the cryogenic targets (hydrogen and deuterium).

Both Hall C spectrometers have similar standard detector packages, each with four scintillator planes[15] used for triggering, a pair of drift chambers[16] used for tracking, and a calorimeter[17] and gas Čerenkov [18, 19] used for electron identification. The trigger setup for this experiment required a minimum of 3/4 hodoscope planes for data readout in each spectrometer. Due to the absence of significant background and the negligible accidental trigger rates at the higher missing momentum settings, the use of additional particle identification (PID) measures was found to have little to no effect on the final cross section.

We measured three central missing momentum settings: $p_r = 80, 580$ and 750 MeV/c. At each of these settings, the electron arm (SHMS) was fixed and the proton arm (HMS) was rotated from smaller to larger angles corresponding to the the lower and higher missing momentum settings, respectively. At these kinematic settings, the 3-momentum transfer covered a range of $2.4 \lesssim |\vec{q}| \lesssim 3.2$ GeV/c which is more than twice the highest neutron recoil momentum (p_r) measured on this experiment. As a result, most of the virtual photon momentum is transferred to the proton which scatters at angles relative to $\vec{q}$ in the range $0.4^o \lesssim \theta_{pq} \lesssim 21.4^o$. At these forward angles and large momentum transferred to the proton, the process where the neutron is struck by the virtual photon is suppressed.

Hydrogen elastic $^1H(e,e'p)$ data was also taken at kinematics close to the deuteron p_r=80 MeV setting for cross-checks with the spectrometer acceptance model using the Hall C Monte Carlo simulation program, SIMC. Additional $^1H(e,e'p)$ data were also taken at three other kinematic settings that covered the SHMS momentum acceptance range for the deuteron and were used for spectrometer optics optimization, momentum calibration and the determination of the spectrometer offsets and kinematic uncertainties[20, 21].

Identical event selection criteria were used for the hydrogen and deuteron data. The criteria were determined by making standard cuts on the spectrometer momentum fraction (δ) to select a region in which the reconstruction optics is well known, a cut to restrict the HMS solid angle acceptance to events that passed directly through the collimator and not by re-scattering from the collimator edges, a missing energy cut (peak $\sim$ 2.22 MeV for the deuteron) to select true $^2H(e,e'p)n$ coincidences, a coincidence time cut to select true coincidence events and not accidentals, a PID cut on the SHMS calorimeter normalized total track energy to select electrons and not other sources of background (mostly pions) and a cut on the reconstructed HMS and SHMS reaction vertices to select events that originated from the same reaction vertex at the target.

The experimental data yields for both hydrogen and deuteron data were normalized by the total charge and corrected for various inefficiencies. For $^2H(e,e'p)n$ the corrections were as follows: tracking efficiencies (98.9%-

HMS, 96.4%-SHMS), total live time (92.3%), proton loss due to nuclear interactions in the HMS (4.7%)[22] and target boiling factors (4.2%)[23]. The values in parentheses were averaged over all data sets.

For $^1H(e,e'p)$, the corrected data yield was compared to SIMC calculations using J. Arrington's proton form factor parametrization[24] to check the spectrometer acceptance model. The ratio of data to simulation yield was determined to be $97.6 \pm 0.3\%$ (statistical uncertainty only). For $^2H(e,e'p)n$, the low missing momentum data ($p_r = 80$ MeV/c) were compared to the Hall A data (See Fig. 1). The good agreement gives us confidence on the measurements made at higher missing momentum settings for which no previous data exist.

The systematic uncertainties of the measured cross sections were determined from normalization[25] and kinematic uncertainties in the beam energy and spectrometer angle/momentum settings. The individual contributions from normalization uncertainties were determined to be: tracking efficiencies (0.40%-HMS, 0.59%-SHMS), target boiling (0.39%), total live time (3.0%) and total charge (2.0%) for an overall normalization uncertainty added in quadrature of 3.7%.

The systematic uncertainties due to our limited knowledge of the beam energy and spectrometer angle/momentum settings were determined point-to-point in (θ_{nq}, p_r) bins for each data set independently, and added in quadrature for overlapping p_r bins of different data sets. For $\theta_{nq} = 35^o, 45^o and 75^o$ (presented on this Letter) the overall kinematic uncertainty varied up to 6.5% for $p_r \leq 1.01$ GeV/c. The overall systematic uncertainty in the cross section was determined by the quadrature sum of the normalization and kinematic uncertainties. This result was then added in quadrature to the statistical uncertainty(25-30% on average) to obtain the final uncertainty in the cross section.

The data were radiatively corrected for each bin in (θ_{nq}, p_r) by multiplying the measured cross sections by the ratio of the calculated particle yield excluding and including radiative effects. The Monte-Carlo code SIMC was used for these calculations with the Deuteron Model by J.M.Laget including FSI [26]. For each bin in (θ_{nq}, p_r), the averaged $^2H(e,e'p)n$ kinematics has been calculated and used in the bin centering correction factor defined as: $f_{bc} \equiv \sigma_{avg.kin}/\bar{\sigma}$, where $\sigma_{avg.kin}$ is the cross section calculated at the averaged kinematics and $\bar{\sigma}$ is the cross section averaged over the kinematic bin.

Both experimental and theoretical reduced cross sections were extracted from the measured and calculated cross sections for each data set independently and subsequently averaged for overlapping bins in p_r. The reduced cross sections are defined as follows:

$$\sigma_{red} \equiv \frac{\sigma_{exp(th)}}{K f_{rec} \sigma_{cc1}} \tag{1}$$

where $\sigma_{exp(th)}$ is the 5-fold experimental (or theoretical) differential cross section $\frac{d^5\sigma}{d\omega d\Omega_e d\Omega_p}$, K is a kinematical factor, f_{rec} is the recoil factor and σ_{cc1} is the de Forest[27] electron-proton off-shell cross section calculated using the form factor parametrization of Ref.[24]. Within the PWIA, σ_{red} corresponds to the proton momentum distribution inside the deuteron.

Figure 1 shows the extracted experimental and theoretical reduced cross sections as a function of neutron recoil momentum p_r for three recoil angle settings at

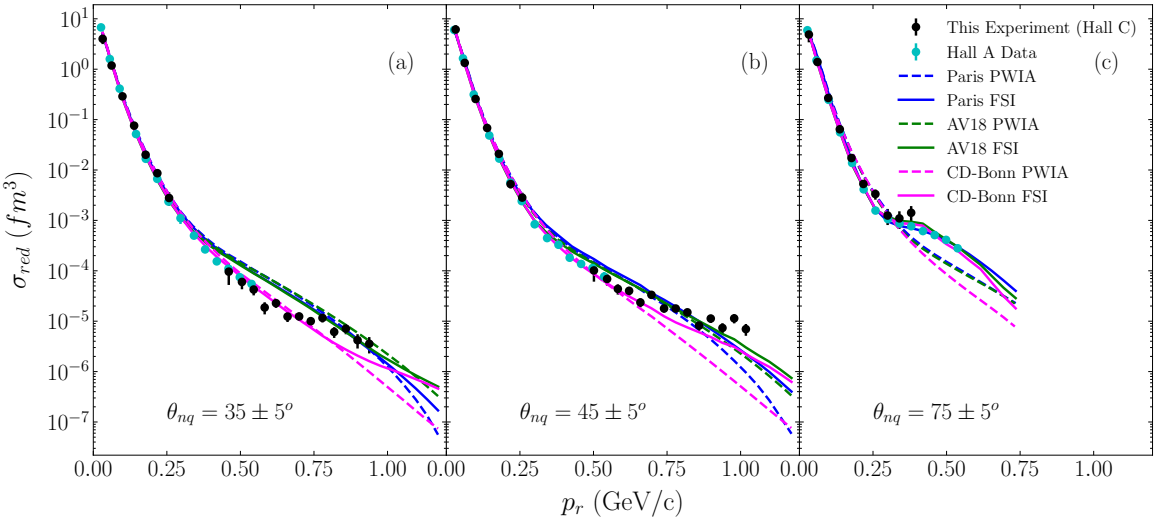

FIG. 1. The reduced cross sections $\sigma_{red}(p_r)$ as a function of neutron recoil momentum p_r are shown in (a)-(c) for recoil angles $\theta_{nq} = 35^o, 45^o$ and 75^o, respectively, with a bin width of $\pm 5^o$. The data is compared to the previous Hall A experiment (cyan) results[14] as well as the theoretical reduced cross sections using the Paris(blue), AV18(green) and CD-Bonn(magenta) NN potentials

$Q^2 = 4.5 \pm 0.5$ (GeV/c)^2. The results from the previous Hall A experiment[14] at a $Q^2 = 3.5 \pm 0.25$ (GeV/c)^2 are plotted as well (cyan). The data are compared to theoretical reduced cross sections using the charge-dependent Bonn (CD-Bonn)[28], Argonne v_{18} (AV18)[29] and Paris[30] NN-potentials. The theoretical calculations for the CD-Bonn (magenta) and AV18 (green) potentials were performed by M. Sargsian[31] and those for the Paris potential (blue) were by J.M. Laget[26].

For all recoil angles shown in Fig. 1 at recoil momenta p_r $\leq$300 MeV/c the cross sections are well reproduced by all models when FSI are included. The agreement at $p_r \leq 300$ MeV/c can be understood from the fact that this region corresponds to the long-range part of the NN potential where the One Pion Exchange Potential (OPEP) is well known and common to all modern potentials.

Beyond p_r ~300 MeV/c at $\theta_{nq} = 35^o$ and 45^o [Figs. 1(a), 1(b)], the Paris and AV18 models significantly differ from the CD-Bonn. In this region, the Paris/AV18 cross sections are dominated by the PWIA and within good agreement of each other up $p_r \sim 700$ MeV/c. The CD-Bonn cross sections in contrast are generally smaller than the Paris/AV18 in this region. In addition for $\theta_{nq} = 35^o$ they are dominated by the PWIA up to $p_r \sim 800$ MeV/c [Fig. 1(a)] while for $\theta_{nq} = 45^o$ FSI start to contribute already above 600 MeV/c [Fig. 1(b)]. The main difference between the CD-Bonn and Paris/AV18 models is the use of Feynman amplitudes in covariant (original) form by the Bonn group as opposed to local (static) approximations of these amplitudes used by Paris/AV18 groups to describe the NN potential. The effect of these local approximations on the NN potential are shown in Fig. 2 of Ref. [28].

At $\theta_{nq} = 75^o$ [Fig. 1(c)] and $p_r > 300$ MeV/c, FSI become the dominant contributions to the cross sections for all models which exhibit a similar behaviour (smaller falloff) that overshadows any possibility of extracting the momentum distributions.

To quantify the discrepancy observed between data and theory in Fig. 1, the ratio of the experimental and theoretical reduced cross sections (σ_{red}) to the deuteron momentum distribution calculated using the CD-Bonn potential ($\sigma_{red}^{\text{CD-Bonn PWIA}}$)[28] is shown in Fig. 2. For $\theta_{nq} = 35^o$ and 45^o [Figs. 2(a),(b)] the data are best described by the CD-Bonn PWIA calculation for recoil momenta up to $p_r \sim 700$ MeV/c and ~ 600 MeV/c, respectively. Furthermore, the agreement between the Halls A and C data solidifies the Hall A approach of selecting a kinematic region where recoil angles are small and FSI are reduced. At larger recoil momenta where the ratio is $R > 1$ and increasing. At $\theta_{nq} = 35^o$ FSI start to dominate for missing moment above typically above 800 MeV/c for the CD-Bonn calculation while the other models predict still relatively small FSI below 900 MeV/c. At $\theta_{nq} = 45^o$ the FSI dominance starts earlier for all models above 800 MeV/c and for the CD-Bonn based calculation above 600 MeV/c.

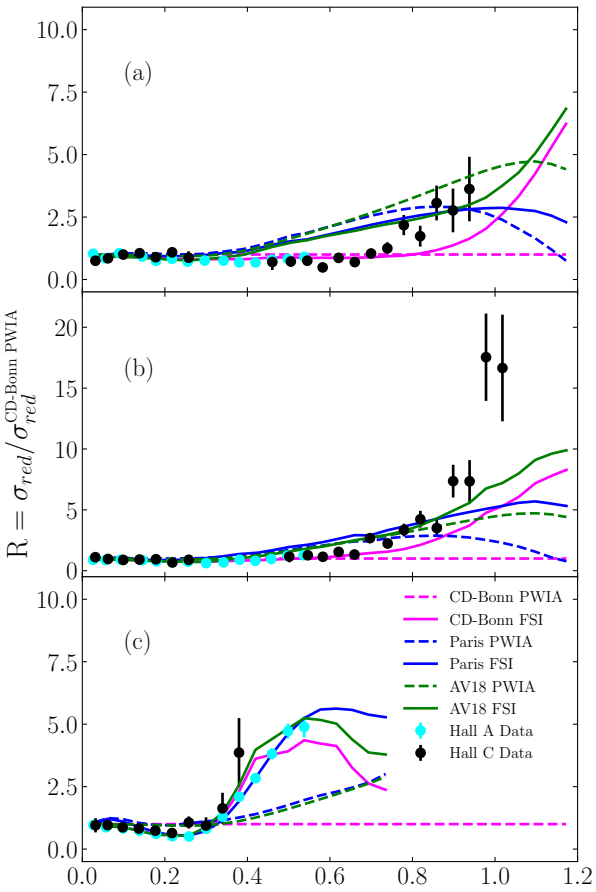

FIG. 2. The ratio $R(p_r) = \sigma_{red}/\sigma_{red}^{\text{CD-Bonn PWIA}}$ is shown in (a)-(c) for $\theta_{nq} = 35^o, 45^o$ and 75^o, respectively, each with a bin width of $\pm 5^o$. The dashed reference (magenta) line refers to CD-Bonn PWIA calculation (or momentum distribution) by which the data and all models are divided.

Overall it is interesting to note that none of the calculations can reproduce the measured p_r dependence above 600 MeV/c in a region where FSI are still relatively small (¡30%). This behavior of the data is new and and additional data in this kinematic region are necessary to improve the statistics.

At $\theta_{nq} = 75^o$ [Fig. 2(c)], FSI are small below $p_r \sim 150$ MeV/c, but do not exactly cancel the PWIA/FSI interference term in the scattering amplitude which results in a small dip in this region in agreement with the data. At $p_r > 300$ MeV/c, the data was statistically limited as our focus was on the smaller recoil angles. The Hall A data, however, shows a reasonable agreement with the

FSI from all models which gives us confidence in our understanding of FSI at the smaller recoil angles.

This experiment extended the previous Hall A cross section measurements on the $^2H(e,e'p)n$ reaction to very high neutron recoil momenta at kinematics where FSI were expected to be small and the cross section was dominated by PWIA and sensitive to the short range part of the deuteron wavefunction. The experimental reduced cross sections were extracted and found to be in good agreement with the Hall A data. Furthermore, the CD-Bonn model was found to be significantly different than the Paris or AV18 models and was able to partially describe the data over a larger range in p_r. At higher missing momentum, however, all models were unable to describe the data.

We acknowledge the outstanding support of the staff of the Accelerator and Physics Divisions at Jefferson Lab as well as the entire Hall C staff, technicians, graduate students and users who took shifts or contributed to the equipment for the Hall C upgrade making all four commissioning experiments possible.

[1] K. S. Egiyan *et al.* (CLAS Collaboration), Observation of nuclear scaling in the $A(e,e^{'})$ reaction at $x_B > 1$, Phys. Rev. C **68**, 014313 (2003).

[2] K. S. Egiyan *et al.* (CLAS Collaboration), Measurement of two- and three-nucleon short-range correlation probabilities in nuclei, Phys. Rev. Lett. **96**, 082501 (2006).

[3] R. Shneor *et al.* (Jefferson Lab Hall A Collaboration), Investigation of proton-proton short-range correlations via the ^{12}C$(e,e^{'}pp)$ reaction, Phys. Rev. Lett. **99**, 072501 (2007).

[4] N. Fomin, D. Higinbotham, M. Sargsian, and P. Solvignon, New results on short-range correlations in nuclei, Annual Review of Nuclear and Particle Science **67**, 129159 (2017).

[5] P. Ulmer *et al.*, Short-Distance Structure of the Deuteron and Reaction Dynamics in ^{2}H(e,e'p)n, https://www.jlab.org/exp_prog/proposals/01/PR01-020.pdf (2001), *Jefferson Lab Proposal E01-020*.

[6] C. Bochna *et al.*, Measurements of deuteron photodisintegration up to 4.0 gev, Phys. Rev. Lett. **81**, 4576 (1998).

[7] E. C. Schulte *et al.*, Measurement of the high energy two-body deuteron photodisintegration differential cross section, Phys. Rev. Lett. **87**, 102302 (2001).

[8] E. C. Schulte *et al.*, High energy angular distribution measurements of the exclusive deuteron photodisintegration reaction, Phys. Rev. C **66**, 042201 (2002).

[9] M. M. Sargsian, Selected Topics in High Energy Semi-Exclusive Electro-Nuclear Reactions, International Journal of Modern Physics E **10**, 405457 (2001).

[10] W. Boeglin and M. Sargsian, Modern studies of the deuteron: From the lab frame to the light front, International Journal of Modern Physics E **24**, 1530003 (2015), https://doi.org/10.1142/S0218301315300039.

[11] L. L. Frankfurt, M. M. Sargsian, and M. I. Strikman, Feynman graphs and generalized eikonal approach to high energy knock-out processes, Phys. Rev. C **56**, 1124 (1997).

[12] P. E. Ulmer *et al.*, ^{2}H$(e,e^{'}p)n$ reaction at high recoil momenta, Phys. Rev. Lett. **89**, 062301 (2002).

[13] K. S. Egiyan *et al.* (CLAS Collaboration), Experimental study of exclusive ^{2}H$(e,e^{'}p)n$ reaction mechanisms at high Q^2, Phys. Rev. Lett. **98**, 262502 (2007).

[14] W. U. Boeglin *et al.* (For the Hall A Collaboration), Probing the high momentum component of the deuteron at high Q^2, Phys. Rev. Lett. **107**, 262501 (2011).

[15] G. Niculescu, I. Niculescu, M. Burton, D. Coquelin, K. Nisson, and T. Jarell, Shms hodoscope scintillator detectors, https://hallcweb.jlab.org/document/howtos/shms_scintillator_hodoscope.pdf.

[16] M. Christy, P. Monaghan, N. Kalantarians, D. Biswas, and M. Long, Shms drift chambers, https://hallcweb.jlab.org/document/howtos/shms_drift_chambers.pdf.

[17] H. Mkrtchyan *et al.*, The lead-glass electromagnetic calorimeters for the magnetic spectrometers in hall c at jefferson lab, Nuclear Instruments and Methods in Physics Research Section A: Accelerators, Spectrometers, Detectors and Associated Equipment **719**, 85100 (2013).

[18] W. Li, *Heavy Gas Cherenkov Detector Construction for Hall C at Thomas Jefferson National Accelerator Facility*, Master's thesis, University of Regina (2012).

[19] D. Day, Preliminary design of the shms noble cerenkov detector, https://hallcweb.jlab.org/DocDB/0009/000933/001/shms-cerv6.pdf.

[20] C. Yero, Update on spectrometer offsets determination using h(e,e'p) elastics (2019), https://hallcweb.jlab.org/DocDB/0010/001036/002/HC_SoftwareMeeting_Oct03_2019_pdf.pdf.

[21] C. Yero, Optics optimization for the d(e,e'p)n experiment [e12-10-003] (2019), https://hallcweb.jlab.org/DocDB/0010/001033/001/d2_optim.pdf.

[22] C. Yero, Proton absorption (2019), https://hallcweb.jlab.org/DocDB/0010/001020/002/ProtonAbsorption_slides.pdf.

[23] C. Yero, Hms target boiling studies (2019), https://hallcweb.jlab.org/DocDB/0010/001023/003/TargetBoiling_v2.pdf.

[24] J. Arrington, Implications of the discrepancy between proton form factor measurements, Phys. Rev. C **69**, 022201 (2004).

[25] Conservative estimates on the systematic uncertainties of the total live and charge were made. Determination of systematics on these quantities is a work in progress. (Private communication with D. Mack).

[26] J. Laget, The electro-disintegration of few body systems revisited, Physics Letters B **609**, 49 (2005).

[27] T. D. Forest, Off-shell electron-nucleon cross sections: The impulse approximation, Nuclear Physics A **392**, 232 (1983).

[28] R. Machleidt, High-precision, charge-dependent bonn nucleon-nucleon potential, Phys. Rev. C **63**, 024001 (2001).

[29] R. B. Wiringa, V. G. J. Stoks, and R. Schiavilla, Accurate nucleon-nucleon potential with charge-independence breaking, Phys. Rev. C **51**, 38 (1995).

[30] M. Lacombe, B. Loiseau, J. M. Richard, R. V. Mau, J. Côté, P. Pirès, and R. de Tourreil, Parametrization of the paris $n-n$ potential, Phys. Rev. C **21**, 861 (1980).

[31] M. M. Sargsian, Large Q^2 electrodisintegration of the deuteron in the virtual nucleon approximation, Phys. Rev. C **82**, 014612 (2010).